



SPACOMM 2022

The Fourteenth International Conference on Advances in Satellite and Space
Communications

ISBN: 978-1-61208-939-3

April 24 - 28, 2022

Barcelona, Spain

SPACOMM 2022 Editors

Timothy Pham, Jet Propulsion Laboratory, USA

SPACOMM 2022

Forward

The Fourteenth International Conference on Advances in Satellite and Space Communications (SPACOMM 2022) continued a series of events to evaluate the state of the art on academia and industry on the satellite, radar, and antennas-based communications bringing together scientists and practitioners with challenging issues, achievements, and lessons learnt.

Significant efforts have been allotted to design and deploy global navigation satellite communications systems, Satellite navigation technologies, applications, and services experience still challenges related to signal processing, security, performance, and accuracy. Theories and practices on system-in-package RF design techniques, filters, passive circuits, microwaves, frequency handling, radars, antennas, and radio communications and radio waves propagation have been implemented. Services based on their use are now available, especially those for global positioning and navigation. For example, it is critical to identify the location of targets or the direction of arrival of any signal for civilians or on-purpose applications; smart antennas and advanced active filters are playing a crucial role. Also, progress has been made for transmission strategies; multiantenna systems can be used to increase the transmission speed without need for more bandwidth or power. Special techniques and strategies have been developed and implemented in electronic warfare target location systems.

We take here the opportunity to warmly thank all the members of the SPACOMM 2022 technical program committee, as well as all the reviewers. The creation of such a high-quality conference program would not have been possible without their involvement. We also kindly thank all the authors who dedicated much of their time and effort to contribute to SPACOMM 2022. We truly believe that, thanks to all these efforts, the final conference program consisted of top-quality contributions. We also thank the members of the SPACOMM 2022 organizing committee for their help in handling the logistics of this event.

SPACOMM 2022 Chairs

SPACOMM 2022 Steering Committee

Timothy T. Pham, Jet Propulsion Laboratory - California Institute of Technology, USA

Stelios Papaharalabos, u-blox Athens, Greece

Oliver Michler, Technical University Dresden, Germany

SPACOMM 2022 Publicity Chairs

Javier Rocher, Universitat Politècnica de València, Spain

Lorena Parra, Universitat Politècnica de València, Spain

SPACOMM 2022 Committee

SPACOMM 2022 Steering Committee

Timothy T. Pham, Jet Propulsion Laboratory - California Institute of Technology, USA
Stelios Papaharalabos, u-blox Athens, Greece
Oliver Michler, Technical University Dresden, Germany

SPACOMM 2022 Publicity Chairs

Javier Rocher, Universitat Politècnica de València, Spain
Lorena Parra, Universitat Politècnica de València, Spain

SPACOMM 2022 Technical Program Committee

Zahir A. Hussein Alsulaimawi, Oregon State University, USA
Suayb S. Arslan, MEF University, Turkey
Michael Atighetchi, Raytheon BBN Technologies, USA
Peter Baumann, Jacobs University, Germany
Yao-Yi Chiang, University of Southern California - Spatial Sciences Institute, USA
Raed S.M Daraghmah, Palestine Technical University, Palestine
Arun Das, Arizona State University, USA
Yiping Duan, Tsinghua University, China
Nour El Madhoun, Laboratoire Sécurité & Système de l'EPITA (LSE), France
Mohamed A. Elshafey, Military Technical College, Cairo, Egypt
Luiz Carlos Gadelha de Souza, Federal University of ABC, Brazil
Gregory Hellbourg, International Center for Radio Astronomy Research | Curtin University, Western Australia
Sundararaja Sitharama Iyengar, Florida International University, USA
Seifallah Jardak, Bristol Research & Innovation Laboratory - Toshiba, UK
Baris Kazar, Oracle America Inc., USA
Mohamed Khalaf-Allah, Technische Universität Dresden, Germany
Adil Hakeem Khan, Nation College of Engineering and Technology, Guna, India
Arash Komae, Southern Illinois University, Carbondale, USA
Fandel Lin, National Cheng Kung University, Taiwan
Pablo Madoery, Universidad Nacional de Córdoba, Argentina
Krešimir Malarić, University of Zagreb, Croatia
Michael P. McGuire, Towson University, USA
Oliver Michler, Technical University Dresden, Germany
Sara Migliorini, Università degli Studi di Verona, Italy
Nelli Mosavi, Johns Hopkins University, USA
Tathagata Mukherjee, The University of Alabama in Huntsville, USA
David N. Amanor, Intel Corporation, USA
Brian Niehoefer, TÜV Informationstechnik GmbH, Germany
Nele Noels, Ghent University, Belgium
W. David Pan, University of Alabama in Huntsville, USA
Krishna Pande, National Chiao Tung University, Taiwan
Cathryn Peoples, Ulster University, UK
Timothy Pham, Jet Propulsion Laboratory, USA

Ermanno Pietrosevoli, The Abdus Salam International Centre for Theoretical Physics (ICTP), Italy
Cong Pu, Marshall University, Huntington, USA
Alexandru Rusu, University Politehnica of Bucharest, Romania
Takeyasu Sakai, Electronic Navigation Research Institute - National Institute of Maritime, Port and
Aviation Technology, Japan
Predrag Spasojevic, Rutgers University, USA
Cristian Lucian Stanciu, University Politehnica of Bucharest, Romania
Veeru Talreja, West Virginia University, USA
Stefanos Vrochidis, Information Technologies Institute, Greece
Tin Vu, Microsoft, USA
Xiao Wang, Boston University, USA
Hong Wei, University of Maryland, USA
Yimin Daniel Zhang, Temple University, USA
Yunfan Gerry Zhang, Independent Researcher, USA

Copyright Information

For your reference, this is the text governing the copyright release for material published by IARIA.

The copyright release is a transfer of publication rights, which allows IARIA and its partners to drive the dissemination of the published material. This allows IARIA to give articles increased visibility via distribution, inclusion in libraries, and arrangements for submission to indexes.

I, the undersigned, declare that the article is original, and that I represent the authors of this article in the copyright release matters. If this work has been done as work-for-hire, I have obtained all necessary clearances to execute a copyright release. I hereby irrevocably transfer exclusive copyright for this material to IARIA. I give IARIA permission to reproduce the work in any media format such as, but not limited to, print, digital, or electronic. I give IARIA permission to distribute the materials without restriction to any institutions or individuals. I give IARIA permission to submit the work for inclusion in article repositories as IARIA sees fit.

I, the undersigned, declare that to the best of my knowledge, the article does not contain libelous or otherwise unlawful contents or invading the right of privacy or infringing on a proprietary right.

Following the copyright release, any circulated version of the article must bear the copyright notice and any header and footer information that IARIA applies to the published article.

IARIA grants royalty-free permission to the authors to disseminate the work, under the above provisions, for any academic, commercial, or industrial use. IARIA grants royalty-free permission to any individuals or institutions to make the article available electronically, online, or in print.

IARIA acknowledges that rights to any algorithm, process, procedure, apparatus, or articles of manufacture remain with the authors and their employers.

I, the undersigned, understand that IARIA will not be liable, in contract, tort (including, without limitation, negligence), pre-contract or other representations (other than fraudulent misrepresentations) or otherwise in connection with the publication of my work.

Exception to the above is made for work-for-hire performed while employed by the government. In that case, copyright to the material remains with the said government. The rightful owners (authors and government entity) grant unlimited and unrestricted permission to IARIA, IARIA's contractors, and IARIA's partners to further distribute the work.

Table of Contents

Alleviating Bundle Throughput Constriction for Delay Tolerant Networking (DTN) Bundles with Software Defined Networking (SDN) 1

Stephanie Booth, Alan Hylton, Rachel Dudukovich, Nadia Kortas, Blake LaFuente, and Brian Tomko

Design of Highly Selective Band-pass Filter with Wide Stop-band using Open Stubs and Spurlines for Satellite Communication (SATCOM) Applications 6

Nitin Muchhal, Mostafa Elkhoully, Kurt Blau, and Shweta Srivastava

Alleviating Bundle Throughput Constriction for Delay Tolerant Networking (DTN) Bundles with Software Defined Networking (SDN)

Stephanie Booth
 NASA Glenn Research Center
 Cleveland, Ohio
 email: stephanie.l.booth@nasa.gov

Alan Hylton
 NASA Goddard Space Flight Center
 Greenbelt, Maryland
 email: alan.g.hylton@nasa.gov

Rachel Dudukovich
 NASA Glenn Research Center
 Cleveland, Ohio
 email: rachel.m.dudukovich@nasa.gov

Nadia Kortas
 NASA Glenn Research Center
 Cleveland, Ohio
 email: nadia.kortas@nasa.gov

Blake LaFuenta
 NASA Glenn Research Center
 Cleveland, Ohio
 email: blake.a.lafuenta@nasa.gov

Brian Tomko
 NASA Glenn Research Center
 Cleveland, Ohio
 email: brian.j.tomko@nasa.gov

Abstract—A load-balancing technique is proposed, executed, and tested against a Delay Tolerant Network (DTN) implementation with well-known characteristics. This would prove that transparently inserting Software Defined Networking (SDN) to achieve load balancing without re-configuring the DTN portion is possible. In addition, two routes were taken to alleviate a DTN bottleneck threat. The first used a P4 networking switch. This manual load-balancing test will balance the incoming packets without the users at the end-points knowing that their original packet destinations and/or sources may have been changed. The second route utilized a High-rate Delay Tolerant Networking (HDTN) receiving node instead of the typical DTN implementation used. Bench-marking results of the DTN implementation receiving node and the HDTN receiving node will be compared.

Index Terms—*Delay Tolerant Networking (DTN); Software Defined Network (SDN); Interplanetary Overlay Network (ION); High-rate Delay Tolerant Networking (HDTN); Space Communications*

I. INTRODUCTION

As space networks expand and increase complexity, bundle (and packet) throughput will also increase. This leads to the idea that individual nodes must be able to handle increased traffic, particularly from multiple sources and to multiple destinations. Consider an example with two nodes. Node 1 is sending bundles, at its processing limit, and likewise node 2 is receiving bundles at its limit. If a third node was introduced to this system sending any number of packets to node 2, then node 2 will be over capacity. In this case, the best-case scenario is that bundles must be re-transmitted. The question becomes how cases like these could be handled at a system level. An approach for future networks to load-balance themselves through a Software Defined Networking (SDN) switch or a High-rate Delay Tolerant Networking (HDTN) capability is outlined in [1].

Space networks are well-known for links featuring high propagation times and intermittent connectivity. These difficulties give rise to Delay Tolerant Networking (DTN), which

is an experimental network protocol designed for this environment. The DTN implementation used in this paper is the Interplanetary Overlay Network (ION), which is NASA's current implementation of delay tolerant networking for space communication applications [2]. Previous work shows ION's performance limitation capabilities where it can process, at most, low-thousands of bundles per second [1]. This provides concerns with scaling networks and limiting throughput. Since ION imposes clear constraints on network performance, it is easy to see noticeable improvement within the system if the load-balancing alleviates bundle throughput.

SDN switches range in capabilities due to hardware configuration limitations and the networking software. For the experiments within this paper, an Aurora 710 networking switch by Netberg was used. This particular switch provides 32 x 100GbE four-lane Quad Small Form-factor Pluggable (QSFP) interfaces with programmable pipelines using the Programming Protocol-Independent Packet Processors (P4) language. The Intel Tofino switching Integrated Circuit (IC) is capable of 3.2T switching and, therefore, will not be a bottleneck in this experiment [3]. ION was configured to transmit bundles over the User Datagram Protocol (UDP), and hence the Aurora 710 P4 networking switch was programmed to seamlessly load balance UDP packets. The authors hasten to add that any protocol, including custom protocols, could have been used.

P4 is one of many different network switch languages that can be used to change how a typical network switch works, but was chosen as it is open-source and has been around since 2013. Prior to the language's first appearance, vendors of data plane devices had total control over any device's functionality. However, now it is possible to implement specific behavior in the network within minutes by avoiding firmware and hardware development. Since P4's initial debut, the language has gone through two major reworks, known as P4₁₄ and P4₁₆

[4]. The Aurora network switch is compatible with both, but P4₁₆ was used for this paper.

Next generation space networks require systems that can handle longer latency times than naturally occur on Earth. HDTN is a performance-optimized implementation of DTN used in this paper, and is optimized for a nearby network of space systems [1]. HDTN is designed with a message bus architecture to attempt to eliminate software bottlenecks caused by shared memory and related locking mechanisms, such as semaphores and mutexes. HDTN decodes bundles and metadata into internal messages to control how data flows through the system.

Figure 1 shows a high level diagram of one of the network components discussed in this paper. Two ION nodes send bundles over UDP to HDTN through the P4 switch. Bundles are received by HDTN's ingress module, which decodes the bundle header to determine the message's desired destination and Time-To-Live (TTL). If there is no route available to reach the destination, bundles are saved to disk by HDTN's storage module. The scheduler determines if a link is available to transfer bundles to another node. HDTN can either send bundles directly through to the egress module, or storage will retain the bundle until it receives a release message. Here would be an example of when bottlenecks of data transmission can pose a problem. If the storage is not large enough, the packets are dropped [5]. In addition, if the receiver is unable to process the data quick enough to handle the two ION nodes, packets can also be lost. For the experiments conducted in this paper, bundles were stored to disk when they were received.

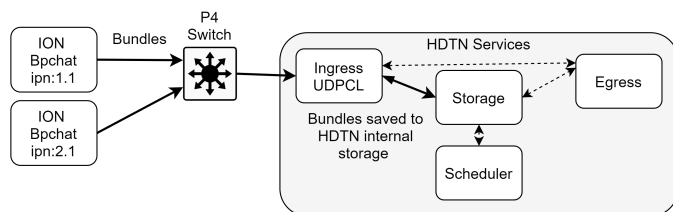


Figure 1. High Level Network Components.

This paper is structured logically to answer these questions regarding continuous data transmission at nodes' capacities. It first mentions the SDN development procedure in Section II. This area lays out the P4 code behind the scenes. Then in Section III, testing starts with placing the SDN switch between two ION nodes to test a small scale load balancing effort. Section IV enhances this effort to balancing multiple DTN nodes with HDTN. And finally, Section V summarizes and concludes the work presented.

II. SDN DEVELOPMENT PROCEDURE

The Aurora 710 networking switch was provided blank, that is, without any inherent protocol support. The switch was first coded in P4 to perform packet switching on Layer 3/Internet Protocol (IP) logical addressing. Once completed, Layer 4 was taken into account. Because bundles were sent over UDP to port 4556, which is normal for DTN, the switch

can easily determine if incoming packets were bundles or not. The network design was straight-forward, and is illustrated in Figure 2. Recall that in ION, node names are numbers; in our case these are the final octets of the node's IP address. Hence Rho, which has IP 10.10.10.1, is node ipn:1.

After basic Layer 3 switching and packet header checks, Network Address Translations (NAT) happen next. To start with, if the final octet of the IP address ends in 10 to 19, its original destination will remain unchanged. However, to load balance the traffic, if the source IP address's final octet is between 20 and 29, then the destination IP will change to the first non-zero digit. For example, if the source IP ends in .20, then its destination IP end is changed from .1 to .2. When reversing the traffic flow, source IP address will be analyzed. If the source IP address does not end in a .1, the source IP address will change back to the original 10.10.10.1 address. See Table I for the NAT rules for traffic on port 4556. All the IP address renaming happens on the networking switch in real time. The checksums were then checked before the packet left the switch and were updated if necessary.

TABLE I
NAT RULES FOR TRAFFIC ON PORT 4556

Original		Modification
IP Source	IP Destination	
10.10.10.[10-19, 100]	10.10.10.1	No change
10.10.10.[20-29, 100]	10.10.10.1	Destination → 10.10.10.2
10.10.10.[30-39, 100]	10.10.10.1	Destination → 10.10.10.3
10.10.10.1	10.10.10.[10-19, 100]	No change
10.10.10.2	10.10.10.[20-29, 100]	Source → 10.10.10.1
10.10.10.3	10.10.10.[30-39, 100]	Source → 10.10.10.1

Once the P4 code was compiled and uploaded to the SDN switch, we were ready to start. We enabled the hardware ports, wrote the switching tables, and manually configured the Address Resolution Protocol (ARP) tables (statically) between the machines. An example of the hardware ports and switching tables are shown in Figures 3 and 4. Each port shown in Figure 3 connects to another computer with a corresponding IP address to Table I. For example, port 1 could be connected to the machine with IP address 10.10.10.100 and port 2 is connected to machine with IP address 10.10.10.1. These addresses might change per test group performed due to computer malfunctions and/or limitations. Figure 4 tells the switch where to send the packet depending on its destination address via port number. Terminology overlaps here where the port number in Figure 3 is the hardware cage and lane number used. The port number in Figure 4 connects with the D_P column for Device Port (logical pipe) in Figure 3.

```
bf-sde> pm show
-----+-----+-----+-----+-----+-----+-----+-----+-----+-----+-----+-----+-----+-----+-----+-----+
PORT | MAC | ID_P | IP | PT | SPEED | FEC | RDY | ADM | OPR | LPBK | FRAMES RX | FRAMES TX | E |
-----+-----+-----+-----+-----+-----+-----+-----+-----+-----+-----+-----+-----+-----+-----+-----+
1/0  | 123/0 | 132 | 12 | 4 | 40G | NONE | YES | ENB | UP | NONE | 213 | 0 | 0 |
2/0  | 22/0 | 140 | 2 | 12 | 40G | NONE | YES | ENB | UP | NONE | 219 | 0 | 0 |
3/0  | 21/0 | 148 | 2 | 20 | 40G | NONE | YES | ENB | UP | NONE | 220 | 0 | 0 |
4/0  | 20/0 | 156 | 2 | 28 | 40G | NONE | YES | ENB | UP | NONE | 216 | 0 | 0 |
5/0  | 19/0 | 164 | 2 | 36 | 40G | NONE | YES | ENB | UP | NONE | 3 | 0 | 0 |
6/0  | 18/0 | 172 | 2 | 44 | 40G | NONE | YES | ENB | UP | NONE | 218 | 0 | 0 |
```

Figure 3. Aurora 710 Hardware Port Diagnostics.

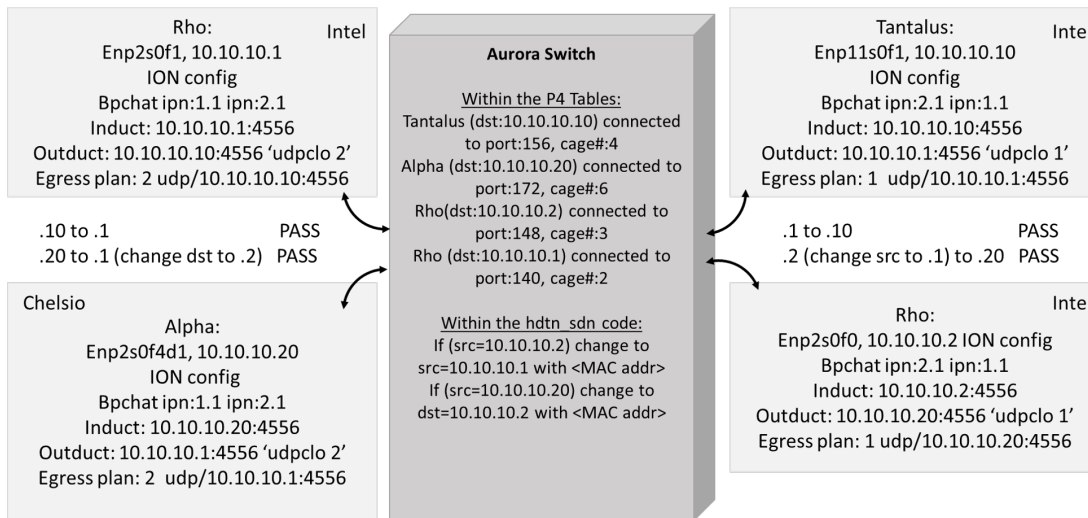


Figure 2. DTN to DTN Roadmap.

```
Table ipv4_host:
--- ipv4_host Dump Start ----
Default Entry:
Entry data (action : NoAction):

pipe.Ingress.ipv4_host entries for action: Ingress.send
hdr.ipv4.dst_addr  port
-----
0x0A0A0A0A        0x0C
0x0A0A0A14        0xAC
0x0A0A0A02        0xA4
0x0A0A0A04        0x84
0x0A0A0A01        0x8C
```

Figure 4. P4 Switching Table for Table Labeled ipv4_host.

Once operational, preliminary tests were conducted of the P4 software using a packet creation software called Scapy via [6] before adding in the DTN implementation. Following Table I, the results showed that the code alters packets only if it was a UDP bundle on port 4556 and all other UDP and TCP packets were switched as normal.

III. SDN MANUALLY LOAD BALANCING ION TO ION

The users from each endpoint should be hidden from the knowledge that their packet destination was altered in the middle of its way to the destination. Hence, between IP addresses ending between .1 and .10, packets are switched without modification. Between .2 and .20 the switch changes the source of .2 to .1 or the destination (if packet is coming from .20) to .1. For a visual of this, see Figure 5. Here, the switch shows that it can manually load balance based on what IP address it came from by changing the destination address. However, due to how Linux's TCP/IP stack is designed and a computer malfunctioning, the DTN implementation tests were broken up between simple switching and modified switching; see Figure 2 for details of each DTN implementation link tested.

The ION implementation's version of bpchat was used to test link connection but was also verified with Wireshark via [7]; this software is often used diagnostically to send text messages over bundles. Because the ARP was not implemented in P4, the ARP tables were manually edited to establish the links. The first test completed used simple UDP switching with an

UDP destination port equaling 4556. This test had no changes to the IP and hardware addresses as expected. See results in Figure 6.

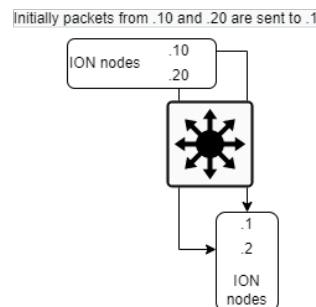


Figure 5. DTN to DTN Load Balancing Overview.

```
Tantalus [.10] -> Rho [.1]
Wireshark capture on Tantalus (shows how packet left):
Frame 1: 99 bytes on wire (792 bits), 99 bytes captured (792 bits) on interface enp11s0f1, id 0
Ethernet II, Src: [redacted], Dst: [redacted]
Internet Protocol Version 4, Src: 10.10.10.10, Dst: 10.10.10.1
User Datagram Protocol, Src Port: 47258, Dst Port: 4556
Bundle Protocol

Wireshark capture on Rho (shows no change):
Frame 1: 99 bytes on wire (792 bits), 99 bytes captured (792 bits) on interface 0
Ethernet II, Src: [redacted], Dst: [redacted]
Internet Protocol Version 4, Src: 10.10.10.10, Dst: 10.10.10.1
User Datagram Protocol, Src Port: 47258, Dst Port: 4556
Bundle Protocol

Rho [.1] -> Tantalus [.10]
Wireshark capture on Rho (shows how packet left):
Frame 2: 99 bytes on wire (792 bits), 99 bytes captured (792 bits) on interface 0
Ethernet II, Src: [redacted], Dst: [redacted]
Internet Protocol Version 4, Src: 10.10.10.1, Dst: 10.10.10.10
User Datagram Protocol, Src Port: 54574, Dst Port: 4556
Bundle Protocol

Wireshark capture on Tantalus (shows no change):
Frame 2: 99 bytes on wire (792 bits), 99 bytes captured (792 bits) on interface enp11s0f1, id 0
Ethernet II, Src: [redacted], Dst: [redacted]
Internet Protocol Version 4, Src: 10.10.10.1, Dst: 10.10.10.10
User Datagram Protocol, Src Port: 54574, Dst Port: 4556
Bundle Protocol

ION bpchat working!
ION bpchat on Rho
slbooth@rho:~/ion-3.7.0/tests/bpchat$ sudo bpchat ipn:1.1 ipn:2.1
from rho to tant
from tant to rho

ION bpchat on Tantalus
slbooth@tantalus:~/ion-3.7.0/tests/bpchat$ sudo bpchat ipn:2.1 ipn:1.1
from rho to tant
from tant to rho
```

Figure 6. Simple Switching with the SDN Switch.

```

Alpha [.20] → Rho [.1]
Will see it on Rho [.2] (IP dst change!) only if UDP dst port 4556
Wireshark capture on Alpha (shows how packet left):
Frame 2: 100 bytes on wire (800 bits), 100 bytes captured (800 bits) on interface 0
Ethernet II, Src: [redacted], Dst: [redacted]
Internet Protocol Version 4, Src: 10.10.10.20, Dst: 10.10.10.1
User Datagram Protocol, Src Port: 57932, Dst Port: 4556
Bundle Protocol

Wireshark capture on Rho (shows the change):
Frame 2: 100 bytes on wire (800 bits), 100 bytes captured (800 bits) on interface 0
Ethernet II, Src: [redacted], Dst: [redacted]
Internet Protocol Version 4, Src: 10.10.10.20, Dst: 10.10.10.2
User Datagram Protocol, Src Port: 57932, Dst Port: 4556
Bundle Protocol

Rho [.2] → Alpha [.20]
Will see it on Alpha [.2] as source Rho [.1] only if UDP dst port 4556
Wireshark capture on Rho (shows how packet left):
Frame 1: 91 bytes on wire (728 bits), 91 bytes captured (728 bits) on interface 0
Ethernet II, Src: [redacted], Dst: [redacted]
Internet Protocol Version 4, Src: 10.10.10.2, Dst: 10.10.10.20
User Datagram Protocol, Src Port: 44734, Dst Port: 4556
Bundle Protocol

Wireshark capture on Alpha (shows the change):
Frame 2: 91 bytes on wire (728 bits), 91 bytes captured (728 bits) on interface 0
Ethernet II, Src: [redacted], Dst: [redacted]
Internet Protocol Version 4, Src: 10.10.10.1, Dst: 10.10.10.20
User Datagram Protocol, Src Port: 44734, Dst Port: 4556
Bundle Protocol

ION bpchat working!
slbooth@rho:~/ion-3.7.0/tests/bpchat$ sudo bpchat ipn:2.1 ipn:1.1
from alpha to rho
from rho to alpha
slbooth@alpha:~/ion-3.7.0/tests/bpchat$ sudo bpchat ipn:1.1 ipn:2.1
from alpha to rho
from rho to alpha
    
```

Figure 7. Modified Switching with the SDN Switch.

The second test required the SDN switch to modify the packets and kept the UDP destination port as 4556. For bpchat to work, it required IPv4 and UDP checksums to be correct at the receiving node. The address changes are shown in Figure 7 and follow Table I.

The last test of the manual load balancing efforts with the Aurora 710 network switch found throughput limitations for each DTN link. This was to give a baseline prior to sending traffic from two DTN nodes to a single recipient DTN node with HDTN. Typical performance-measuring tools for DTN, and particularly ION, include bpdriver and bpsink, which can send fixed numbers of bundles or stream bundle continuously. Both are designed to work as quickly as possible.

These results are shown in Table II. At 1000 bundles the TTL value was hit. We recall that in the context of DTN, TTL

TABLE II
PRELIMINARY DTN TO DTN BASELINE RESULTS

Tx Computer	Rx Computer	Status
Rho	Eta	
Stopping bpdriver. Total bundles: 100 Time (seconds): 0.535 Total bytes: 100000 Throughput (Mbps): 1.495	Stopping bpcounter; bundles received: 100 Time (seconds): 9.486 Total bytes: 100000 Throughput (Mbps): 0.084	PASS
Stopping bpdriver. Total bundles: 1000 Time (seconds): 5.338 Total bytes: 1000000 Throughput (Mbps): 1.499	Stopping bpcounter; bundles received: 438 Time (seconds): 20.130 Total bytes: 438000 Throughput (Mbps): 0.174	FAIL
Omicron	Eta	
Stopping bpdriver. Total bundles: 100 Time (seconds): 0.558 Total bytes: 100000 Throughput (Mbps): 1.433	Stopping bpcounter; bundles received: 100 Time (seconds): 12.765 Total bytes: 100000 Throughput (Mbps): 0.063	PASS
Stopping bpdriver. Total bundles: 1000 Time (seconds): 2.656 Total bytes: 1000000 Throughput (Mbps): 3.012	Stopping bpcounter; bundles received: 810 Time (seconds): 23.921 Total bytes: 810000 Throughput (Mbps): 0.271	FAIL

is not hop-based, but rather time-based. The tool bpdriver uses a default value of 30 seconds. The SDN switch was able to send each packet through but the destination DTN node could not process as many before the TTL expired. This shows that the DTN implementation used is asymmetric with itself and that in this scenario for 1000 bundles, a node to node link fails. In addition, the results show that the network works loss-free when the nodes are not at their maximum capacity. We will be using the 1000 bundle case, which fails here, to compare against HDTN.

IV. BALANCING MULTIPLE DTN NODES WITH HDTN

The DTN implementation transmitting machine names for these tests are named Rho (with IP address ending in .1) and Omicron (with IP address ending in .2). The HDTN node resides on Eta with an IP address of 10.10.10.100. The Aurora 710 network switch will be between the ION nodes and the HDTN node. Here the HDTN node should only see packets from 10.10.10.1 and therefore will be listening for only that IP, as shown in Figure 8.

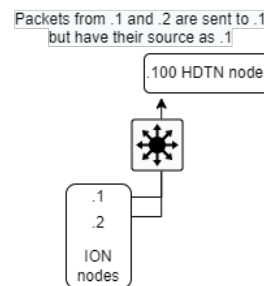


Figure 8. DTN to HDTN Load Balancing Overview.

The HDTN node was configured first to non-volatile storage. Once results were received, bpsink capabilities were tested. No differences of the results proved one configuration was more ideal than the other for these tests with ION.

For a preliminary test of DTN to HDTN, the same test of Table II was conducted except Eta was configured with HDTN. The results brought forth all successes for both ION node links. In addition, when both ION nodes were transmitting 1000 bundles, the HDTN node received all as shown in Table III. Since the previous results of the DTN implementation used had failures (as described in Section III), the PASS results for HDTN under the same conditions are prodigious.

The ION's bpdriver sends its first bundle twice which does not pose counting issues with its counterpart, bpcounter. Since HDTN counts every packet going to storage, even if it is a duplicate, it counts that first packet from both transmitting DTN nodes. This results in the extra two packets counted at the receiver.

TABLE III
DTN TO HDTN TEST RESULTS

Tx Computer	Rx Computer	Status
Rho -hdtm_host1.rc Omicron -hdtm_benchmark1.rc @rho: bpdriver 100 ipn:1.1 ipn:2.1 -1000 t30 Stopping bpdriver. Total bundles: 100 Time (seconds): 0.580 Total bytes: 1000000 Throughput (Mbps): 1.378 @omicron: bpdriver 200 ipn:1.1 ipn:2.1 -1000 t30 Stopping bpdriver. Total bundles: 200 Time (seconds): 0.782 Total bytes: 2000000 Throughput (Mbps): 2.046	Eta ./runscript.sh Only to Storage @eta: hdtm m_bundleCountStorage: 302 m_bundleCountEgress: 0 m_bundleCount: 302 m_bundleData: 312083	PASS
@rho: bpdriver 1000 ipn:1.1 ipn:2.1 -1000 t30 Stopping bpdriver. Total bundles: 1000 Time (seconds): 2.565 Total bytes: 1000000 Throughput (Mbps): 3.119 @omicron: bpdriver 1000 ipn:1.1 ipn:2.1 -1000 t30 Stopping bpdriver. Total bundles: 1000 Time (seconds): 3.109 Total bytes: 1000000 Throughput (Mbps): 2.573	@eta: hdtm m_bundleCountStorage: 2002 m_bundleCountEgress: 0 m_bundleCount: 2002 m_bundleData: 2083906	PASS

V. CONCLUSION

With increasing network throughput and capability needs, bottlenecks are important to avoid. Therefore, it is crucial to circumvent performance restrictions of the network. Thankfully, some options have been found for DTN implementation nodes. Manually load balancing packets with a SDN switch and/or using an HDTN receiver node instead are both viable options for the modern network system.

A benefit to utilizing a SDN switch is that it can handle many different types of networking protocols at line rates. This would enable current and future networks in space to be harnessed with one simple device. The downside is that a SDN switch is not an all-in-one solution since it is unable to create packets to be sent. This would be where a HDTN node plays a key role. It is designed to work with the long latencies and intermittent connections in space. Since its framework is light, it can process and send much faster than current DTN implementations i.e. ION. However, HDTN is a newer implementation that is still in the process of interoperability testing with other DTN implementations such as ION and DTNME. While HDTN is a complete bundle agent, there is a smaller subset of applications and features compared to the larger implementations that have been in use longer. Due to HDTN being still new, it uses modern dependencies and programming techniques. An ideal scenario would be to make use of both, a HDTN and a SDN switch, at each node. This will enable a very intelligent, fast, and expansion-enabled network.

SDN development continues to provide solutions to 100Gbps data rates for HDTN. Current research in teaching the Aurora network switch platform how to automatically load balance traffic between ports without the need of the IP

changes hard-coded into the P4 code continues. In addition, future work will incorporate the bundle egress to neighboring node and finding limitations to HDTN’s capabilities.

REFERENCES

- [1] A. Hylton, D. Raible, and G. Clark, “A delay tolerant networking-based approach to a high data rate architecture for spacecraft,” *IEEE Aerospace Conference*, pp. 1–10, 2019.
- [2] NASA, “Interplanetary overlay network additional information,” accessed: April 2022. [Online]. Available: https://www.nasa.gov/directorates/heo/scan/engineering/technology/disruption_tolerant_networking_software_options_ion
- [3] Netberg, “Aurora 710,” accessed: February 2022. [Online]. Available: <https://netbergtw.com/products/aurora-710/>
- [4] Open Networking Foundations ONF. (2021) P4 open source programming language. Accessed: April 2022. [Online]. Available: www.p4.org
- [5] A. Hylton et al., “New horizons for a practical and performance-optimized solar system internet,” *IEEE Aerospace Conference*, pp. 1–15, 2022.
- [6] Scapy. Accessed: April 2022. [Online]. Available: <https://scapy.net/>
- [7] Wireshark. Accessed: April 2022. [Online]. Available: <https://www.wireshark.org/>

Design of Highly Selective Band Pass Filter with Wide Stop-band using Open Stubs and Spurlines for Satellite Communication (SATCOM) Applications

Nitin Muchhal¹, Mostafa Elkhoully¹, Kurt Blau², Shweta Srivastava³

¹ Fraunhofer Institute for Integrated Circuits IIS, Am Wolfsmantel 33, 91058 Erlangen, Germany
{firstname.lastname@iis.fraunhofer.de}

² Technische Universität Ilmenau, P.O.B. 100565, D-98684 Ilmenau, Germany
{firstname.lastname@tu-ilmenau.de}

³Jaypee Institute of Information Technology, Noida 201309, India
{firstname.lastname@jiit.ac.in}

Abstract - A miniaturized selective composite microstrip Band Pass Filter (BPF) with a 3-dB fractional bandwidth of 52.5% (14.2 GHz to 24.5 GHz) with wide upper stop-band for satellite communication (SATCOM) application is proposed. The design consists of a composite BPF implanted with a pair of quarter-wavelength open-circuited stub and spurline. These elements are combined to form a miniaturized filter with a compact occupied area of $0.72\lambda_g \times 0.55\lambda_g$ ($\approx 0.26 \text{ cm}^2$). The filter is simulated on 0.008" (0.203 mm) Rogers 4003C with dielectric constant, $\epsilon_r=3.55$ using commercial full-wave electromagnetic simulator HFSS v16. Simulated results show that BPF has resonant frequency (f_0) as 14.2 GHz and wide ($>3f_0$) stop band without increasing the circuit size. Further, Spurline behaves as notch filter to suppress the first harmonics (or second pass band) of the proposed BPF.

Keywords- Composite BPF; Open Stub; Spurline; Harmonic Suppression; SATCOM

I. INTRODUCTION

Band Pass Filters (BPFs) have found numerous applications in satellite communication and play a vital role in several microwave and Radio Frequency (RF) applications. A high filtering performance, compact size, wide bandwidth, low insertion loss, wide upper stop-band and low cost are amongst the desired criteria while designing a band-pass filter [1]. In recent time, a significant amount of research work has been going on to design a compact BPF with high selectivity and good stop band performance for Ku/K band applications. Due to scarcity of the bandwidth in lower bands and availability in higher bands, the Ku/K band has become very popular for various satellite communication (SATCOM) applications [2].

Significant studies have been done over the past few years on the design of wideband band pass filters for Ku/K frequency bands using microstrip and Substrate Integrated Waveguide (SIW) [3] technology. Xu et al. [4] projected a Ku band BPF using folded feedlines and quarter-wavelength stepped-impedance resonators to generate multiple coupling paths. Lin et al. [5] proposed a compact novel K band BPF based on

Photonic Band Gap (PBG) structure. Owing to its slow-wave characteristics, the PBG structure reduces the filter size to one-tenth of conventional filters with spurious free response and deep attenuation level. The filter design cascaded several PBG structures introducing a coupling gap. Recently, Navya et al. [6] proposed the design of a low-profile and broad band BPF for Ku band satellite applications which consisted of four $\lambda/4$ transmission lines and two feed lines to connect the resonating lines. In addition, selective band-pass filters for Ku and K bands have been reported by [7] using folded SIW technology incorporating E shape slot in the middle septum. Also, a wideband band-pass filter for Ku band was proposed by [8] using multi-mode resonator Substrate Integrated Waveguide (SIW) technology. Nonetheless, these filters suffered from fabrication complexity due to metallic vias. Further, stop-band response was not very satisfactory. In the past, various researchers have proposed band pass filters, but either the design was quite complex with large size or it suffered from poor selectivity or poor stop band. The present work utilizes the expediency of open stubs and spurline with a composite band pass filter for realizing miniaturized selective band pass filter with wide stop-band. Also, the proposed filter is very easy to fabricate. The designs are simulated using electromagnetic (EM) simulator High Frequency Structure Simulation (HFSS) v.16 software [9].

Section I explains the introduction and literature review. The rest of the paper is structured as follows. Section II explains the design of the composite band-pass filter by combining a low pass and high pass filter. Section III shows the effect of adding open stub on the composite band pass filter for better selectivity. Section IV discusses the effect of adding spurlines for enhancing stop band performance and, finally, Section V presents the conclusion of the proposed work.

II. DESIGN OF THE COMPOSITE BAND PASS FILTER

A wideband BPF can be designed by cascade of a Low Pass Filter (LPF) and a High Pass Filter (HPF) [10], as shown in Figure 1. In this contribution, a stepped impedance structure has been used to design the LPF section as it occupies less area. The function of stepped impedance LPF is to attenuate the second pass-band (harmonics) in the upper stop-band. For attaining the high-pass characteristic, quarter-wave long short-circuited stubs are tapped to the high-impedance sections of the low-pass filter to insert attenuation poles at DC. The objective of the proposed band pass filter is to achieve high selectivity and roll off rate.

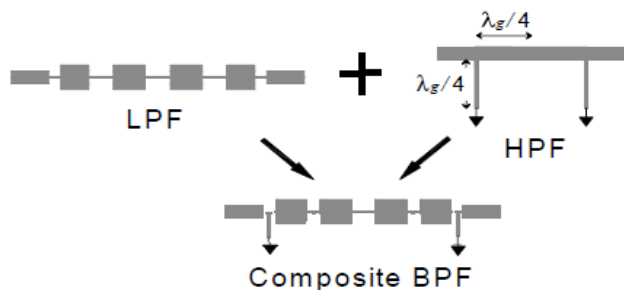


Figure 1. Development of the proposed composite BPF

A. Design of Maximally Flat (Butterworth) Low Pass Filter (LPF)

A butterworth filter has advantage of having more linear phase response in the pass-band thereby able to provide better group delay performance. The column 2 gives element value (g)[10] for maximally flat LPF for N=5. The width and lengths of hi –low impedance sections for maximally flat Low Pass filter (LPF) with cutoff frequency (f_c) = 24 GHz, Filter order (N) = 5, substrate RT Roger 4003 (ϵ_r = 3.55) and substrate height (h) = 0.203 mm is calculated using [11] and is given below in table 1. We have considered Z_l (low impedance value) = 20 Ω , Z_h (high impedance value) =120 Ω , and characteristic impedance, R_o =50 Ω . The electrical length (βl) for C is found using expression $\frac{C}{R_o} \times Z_l$ and for L, it is given as $\frac{L}{Z_h} \times R_o$. The overall dimensions of LPF are: Length, L = 4.4 mm and Width, W = 4.0 mm.

TABLE 1. TABLE TO CALCULATE DIMENSIONS OF LPF

S. No.	Element Value (g)	Z(Ω)	βl (in degree)	L (length in mm)	W (width in mm)
1	$g_1 = 0.5176$ (C1)	20	11.86	$L_2 = 0.25$	$W_2 = 1.96$
2	$g_2 = 1.618$ (L2)	120	38.63	$L_3 = 0.85$	$W_3 = 0.085$
3	$g_3 = 2.0$ (C3)	20	45.86	$L_4 = 0.92$	$W_4 = 1.96$
4	$g_4 = 1.618$ (L4)	120	38.63	$L_3 = 0.85$	$W_3 = 0.085$
5	$g_5 = 0.618$ (C5)	20	14.17	$L_2 = 0.28$	$W_2 = 1.96$
6	$g_6 = 1.0$	50	50	$L_1 = 0.60$	$W_1 = 0.55$

Figure 2 depicts the structure of LPF with calculated dimension.

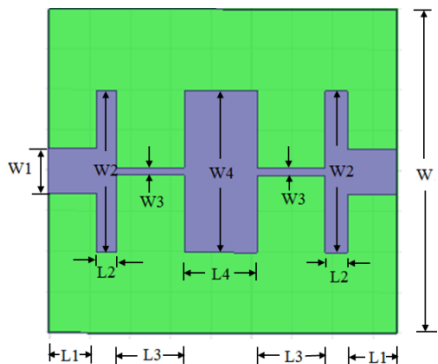


Figure 2. Stepped Impedance Low pass filter

Figure 3 shows the frequency response of LPF. From the graph, it is clear that the LPF possess cutoff frequency of 24 GHz.

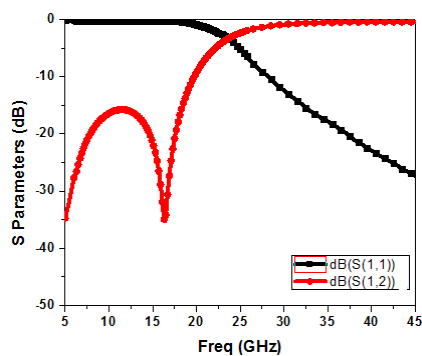


Figure 3. Frequency response of Low pass filter

B. Shorted Stub as High Pass Filter (HPF)

To realize the lower frequency stop-band, quarter-wave short circuited stubs are used with metallic via at the open end of the stub which acts as HPF section of the composite BPF. The length of shorted stub is $\lambda_g/4$ (λ_g : guided wavelength) which turns out to be 1.8 mm for lower cutoff frequency (f_1).

C. Design of Composite Band Pass Filter

To design a composite band pass filter, a High Pass Filtering (HPF) section need to be combined with Low Pass Filtering (LPF) section. The quarter wavelength ($\lambda_g/4$) long short circuited stubs act as HPF. After examining various orientations of shorted stubs, it was found that the shorted stubs placed in alternating positions as shown in Figure 4, gave satisfactory

response. The value of various design parameters are as follows: diameter (D) =0.25 mm, width (W5) = 0.5 mm and length (L5) = 2.6 mm. The overall dimension of the filter is 6 mm x 4.4 mm.

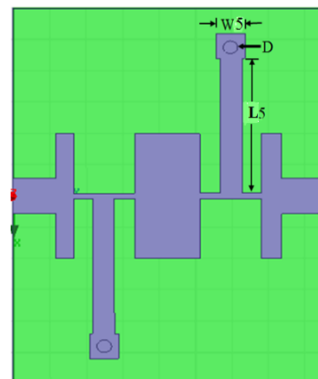


Figure 4. Composite Band-pass filter

Figure 5 depicts the frequency response of the composite BPF. From graph it can be seen that the filter center frequency (f_0) is 18.5 GHz with % Fractional Bandwidth (FBW) of 48%. Further, there appears first harmonic placed near $2f_0$ in the stop band which results in poor stopband performance. Also, the selectivity of the filter is quite poor.

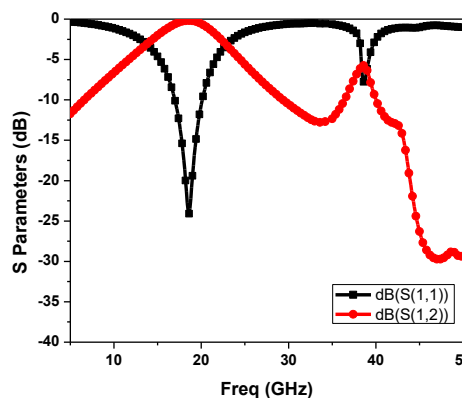


Figure 5. Frequency response of Composite Band-pass Filter

III. COMPOSITE BAND PASS FILTER INTEGRATED WITH OPEN STUBS

To improve the stop band performance and enhance the selectivity of the proposed elliptic filter, open stubs of length $\lambda_g/4$ are placed opposite to the shorted stubs, as shown in Figure 6.

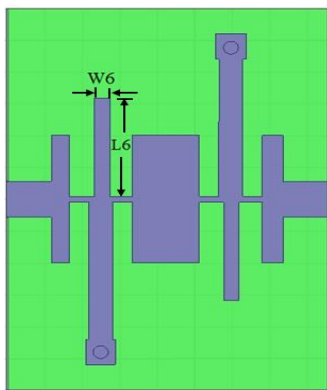


Figure 6. Band-pass Filter with open stubs

To generate a band notch in an Ultra-Wide Band (UWB) BPF, Shaman et al. [12] has proposed the concept of embedded open-circuit stub. The notch effect occurs when the length of open stub is quarter wavelength long [13]. The resonant behavior of $\lambda_g/4$ open-stub can be explained by the equivalent circuit as shown in Figure 7.

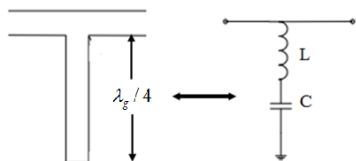


Figure 7. Equivalent circuit of open stub

From the transmission line theory, input impedance for the open-stub is given as:

$$Z_{in} = -jZ_0 \cot \beta l \quad (1)$$

From (1), the impedance of open-sub is low at integer multiple ($n \lambda_g/4$) of resonant frequency thus achieving band-stop or notch characteristics. Also, open stub introduces one Transmission Zero (TZ) augmenting the selectivity of the filter by suppressing the undesired harmonic [14]. The length of the open stub to suppress first spurious responses (located near twice of the fundamental frequency) is calculated to be: $L6=1.55$ mm. The width $W6$ is kept at 0.30 mm. Figure 8 depicts the frequency response of composite BPF embedded with open stubs. From the curve, it is apparent that the center frequency (f_0) of the band pass filter is 19.6 GHz with FBW calculated to be 54.6%.

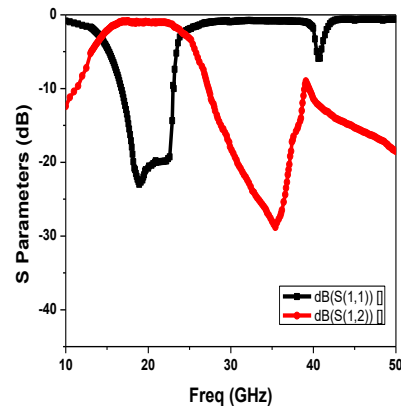


Figure 8. Frequency response of band pass filter with open stubs

Also it is evident from frequency response that the first harmonic (near $2f_0$) is suppressed up to -10 dB with the addition of open stubs, but still stop band performance is not satisfactory.

IV. COMPOSITE BAND PASS FILTER INTEGRATED WITH OPEN STUBS AND SPURLINE

Generally, by cascading additional open stubs into microstrip filter, a wider and a deeper rejection can be achieved. The drawback of this method is high insertion loss in the passband and increased circuit size. A spurline is realized by etching L shape slot on microstrip line exhibiting band-stop (notch) characteristics and also used for further suppressing the harmonics [15][16]. The spur-line filter consists of coupling between two microstrip lines. Figure 9 shows a spur-line filter configuration. Here, 'A' is the length of the spur-line and B is width of the microstrip line.

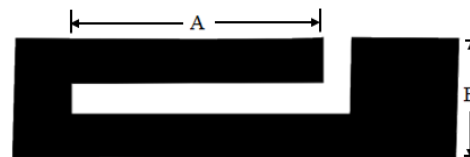


Figure 9. Structure of spurline

Figure 10 shows the structure of the proposed band pass filter incorporating open stubs and spurline. All the dimensions in this layout have been mentioned earlier.

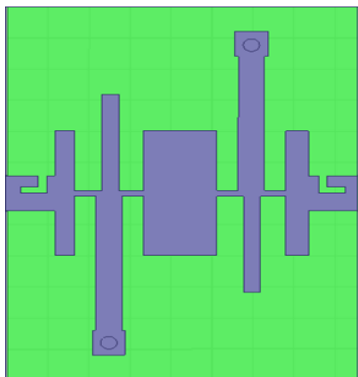


Figure 10. Band pass filter with open stub and spurline

Figure 11 shows the parametric analysis of spurline for various lengths. The length of spurline (A) is calculated by using parametric analysis and it is found that first harmonic ($f_0 = 38.5$ GHz) is well suppressed below -20 dB for spurline length (A) equal to 0.75 mm.

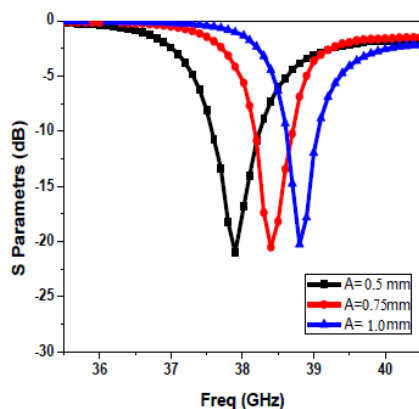


Figure 11. Parametric analysis of spurline for various lengths

Figure 12 shows the frequency response of final proposed band pass filter with open stubs and spurline. It is evident from the response that filter has pass-band from 14.2 GHz to 24.5 GHz with center frequency (f_0) at 19.2 GHz and % FBW calculated to be 52.5% . As can be seen from Figure 12, that additional attenuation is achieved at the first harmonic frequency by the incorporation of the spur line without increasing the circuit size. The harmonic at 38.5 GHz ($2f_0$) is suppressed from -10 dB to -22 dB with the spurline band-stop filter (BSF).

Hence, an improvement in suppression of 12 dB is achieved and out-of-band rejection level is ≥ 20 dB.

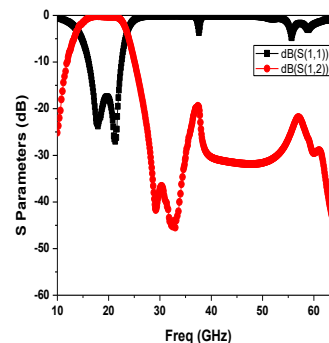


Figure 12. Frequency response of band pass filter with open stub and spurline

V. CONCLUSION

In this paper, a microstrip composite BPF is proposed and simulated using shunt open stubs and spurlines. Basically, open-stub section helps in achieving a wide rejection bandwidth. Further, Spurline with its inherently compact characteristics is inserted on input/output feed-lines that introduce attenuation pole to further suppress the higher harmonic mode resulting in better rejection performance without increasing the size. The proposed filter has merit of compact size with good filtering properties and can be useful for various SATCOM applications.

ACKNOWLEDGEMENT

This work was carried out during the tenure of an ‘ERCIM (The European Research Consortium for Informatics and Mathematics) Alain Bensoussan Fellowship’ programme. Founded in 1988, ERCIM has members from leading European information technology and mathematics research establishments from 18 countries with head office in France.

REFERENCES

- [1] J. S. Hong and, M.J. Lancaster “Microstrip Filters for RF/Microwave Applications”, 2nd Edition, John Wiley & Sons Ltd, 2011.
- [2] M. A Elkhoully et al., “Standardized testing conditions for satellite communications on-the-move (SOTM) terminals”, International Journal of Satellite Communications and Networking, vol 37 3, pp 163-182, June 2019.
- [3] N. Muchhal and S. Srivastava, "Review of recent trends on miniaturization of substrate integrated waveguide (SIW) components," 3rd International Conference on Computational Intelligence & Communication Technology (CICT), India, 2017, pp. 1-6.
- [4] X. Hong, H. Zhang and H. Tang, "Compact Bandpass Filter with Multiple Coupling Paths in Limited Space for Ku-Band Application," in IEEE Microwave and Wireless Components Letters, vol. 27, no. 3, pp. 251-253, March 2017.
- [5] L. Haili, M. Junfa and L. Jianyu, “A Novel compact K band PBG microstrip structure band-pass filter”, International Journal of Electronics, vol. 92, pp. 467-471, 2005.

- [6] A. Navya, G. Immadi, and V. N. Madhavareddy, "A Low-Profile Wideband BPF for Ku Band Applications," *Progress in Electromagnetics Research Letters*, vol. 100, pp. 127-135, 2021.
- [7] N. Muchhal, A. Chakraborty, V. Manoj, and S. Srivastava, "Slotted Folded Substrate Integrated Waveguide Band Pass Filter with Enhanced Bandwidth for Ku/K Band Applications", *Progress in Electromagnetics Research-M*, vol. 70, pp. 51-60, 2018.
- [8] N. Muchhal and S. Srivastava, "Design of Compact and Wideband Comb shape SIW Multimode Resonator Band Pass filter", *International Journal of RF and Microwave Computer-Aided Engineering*, vol 29 (9), pp. 1-9, April 2019.
- [9] User Manual Ansys Inc. High frequency structure simulator (HFSS) software ver. 16.
- [10] C. L. Hsu, H. Fu, and J. K. Kuo, "Microstrip bandpass filters for Ultra-Wideband (UWB) wireless communications," *IEEE MTT-S International Microwave Symposium Digest*, CA, USA, 2005, pp. 679-682
- [11] G. L. Matthaei, L. Young, and E. M. T. Jones, "Microwave Filters, Impedance-Matching Networks, and Coupling Structures", Artech House, Dedham, Mass., 1980.
- [12] H. Shaman and J. S. Hong., "Ultra-Wideband (UWB) Bandpass Filter with Embedded Band Notch Structures," in *IEEE Microwave and Wireless Components Letters*, vol. 17, no. 3, pp. 193-195, March 2007.
- [13] S. Yang, "A compact dual-band bandstop filter having one spurline and two embedded open stubs", *Journal of Electrical Systems and Information Technology (Elsevier)*, vol. 3(2), pp. 314-319, Sept 2016.
- [14] A. I Harikrishnan., S. Mridula and P. Mohanan, "Stub loaded hexagonal open loop band pass filter with improved selectivity," 2019 URSI Asia-Pacific Radio Science Conference (AP-RASC), N. Delhi 2019, pp. 1-4.
- [15] R. N. Bates, "Design of microstrip spurline band-stop filters", *IEE Journal on Microwaves, Optics and Acoustics*, vol. 1(6), 209-214, 1977 doi:10.1049/tj-moa.1977.0029 .
- [16] T. Das, S. Chatterjee, "Harmonic Suppression by Using T-shaped Spur-Line in a Compact Hairpin-Line Bandpass Filter", *Radio Engineering*, vol. 30(2), pp 295-303, June 2021.